JACS
JOURNAL OF THE AMERICAN CHEMICAL SOCIETY
Article
pubs.acs.org/JACS

Carbon Monoxide Induced Reductive Elimination of Disulfide in an N-Heterocyclic Carbene (NHC)/ Thiolate Dinitrosyl Iron Complex (DNIC)

Randara Pulukkody,[†] Samuel J. Kyran,[†] Ryan D. Bethel,[†] Chung-Hung Hsieh, Michael B. Hall, Donald J. Darensbourg, and Marcetta Y. Darensbourg*

Department of Chemistry, Texas A & M University, College Station, Texas 77843, United States

Supporting Information

ABSTRACT: Dinitrosyliron complexes (DNICs) are organometallic-like compounds of biological significance in that they appear *in vivo* as products of NO degradation of iron−sulfur clusters; synthetic analogues have potential as NO storage and releasing agents. Their reactivity is expected to depend on ancillary ligands and the redox level of the distinctive $Fe(NO)_2$ unit: paramagnetic $\{Fe(NO)_2\}^9$, diamagnetic dimerized forms of $\{Fe(NO)_2\}^9$ and diamagnetic $\{Fe(NO)_2\}^{10}$ DNICs (Enemark−Feltham notation). The typical biological ligands cysteine and glutathione themselves are subject to thiolate-disulfide redox processes, which when coupled to DNICs may lead to intricate redox processes involving iron, NO, and $RS^-/RS\bullet$. Making use of an N-heterocyclic carbene-stabilized DNIC, $(NHC)(RS)Fe(NO)_2$, we have explored the DNIC-promoted $RS^-/RS\bullet$ oxidation in the presence of added CO wherein oxidized $\{Fe(NO)_2\}^9$ is reduced to $\{Fe(NO)_2\}^{10}$ through carbon monoxide (CO)/RS• ligand substitution. Kinetic studies indicate a bimolecular process, rate = k $[Fe(NO)_2]^1[CO]^1$, and activation parameters derived from k_{obs} dependence on temperature similarly indicate an associative mechanism. This mechanism is further defined by density functional theory computations. Computational results indicate a unique role for the delocalized frontier molecular orbitals of the $Fe(NO)_2$ unit, permitting ligand exchange of RS• and CO through an initial side-on approach of CO to the electron-rich N−Fe−N site, ultimately resulting in a 5-coordinate, 19-electron intermediate with elongated Fe−SR bond and with the NO ligands accommodating the excess charge.

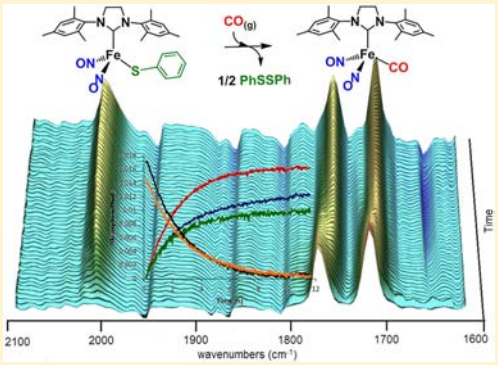

INTRODUCTION

The biologically relevant organoiron moieties identified in the active sites of hydrogenases that contain diatomic ligands CO and CN^- bound to iron have attracted organometallic chemists to the realm of biomimetic synthesis, traditionally relegated to classical coordination chemistry. Similarly, the remarkable $Fe(NO)_2$ unit, reputed to have an active role in controlling NO levels in biology[1−3] and commonly revealed as four-coordinate tetrahedral dinitrosyl iron complexes (DNICs),[4−6] harkens to the interphase of organometallic and classical coordination chemistry. For the former, neutral $L_2Fe(NO)_2$ complexes (L = CO, PR_3, imidazole, or N-heterocyclic carbenes) yield the diamagnetic irondinitrosyl unit to be isoelectronic with $Fe^0(CO)_3$, for which myriad mononuclear $L_2Fe^0(CO)_3$ complexes are known.[7−10] A one-electron-oxidized form of $Fe(NO)_2$ is found in neutral $L(X)Fe(NO)_2$ and anionic $X_2Fe(NO)_2^-$ DNICs which are $S = 1/2$, paramagnetic species, typically identified in biology by a prominent EPR signal at 2.03 and ligated with X = cysteine or glutathione thiolate S-donors and L = histidine N-donors.[1,11,12] An electron-tracking scheme devised by Enemark and Feltham (the E−F notation)[13] avoids the thorny issue of iron oxidation state in the presence of the highly delocalizing NO ligand and assigns the oxidized DNICs to an electron count of $\{Fe(NO)_2\}^9$ and the reduced form, $\{Fe(NO)_2\}^{10}$. With substantial evidence, the $\{Fe(NO)_2\}^9$ unit is posited to be nature designed for NO storage and transport,[1,6,14] of greater stability than the bioorganic RSNO analogue[15] which has traditionally been assumed to stabilize the highly reactive NO radical for delivery to various physiological process centers.

In the past decade, extensive synthetic and biomimetic progress has been made in the DNIC area, including detailed investigations of electronic properties "beyond the E−F notation",[16−18] the establishment of requirements for NO release from DNICs,[19] discovery of DNICs of higher coordination number,[20−22] assessment of potential for photo-therapeutic applications,[23,24] etc. To our knowledge there is only one example of an X-ray crystal structure of a protein-bound DNIC.[25] This was derived from exposing glutathione-S-transferase (GST) to an exogeneously formed $(glutathione)_2Fe(NO)_2$. Enzyme recognition of the modified glutathione resulted in tyrosine replacement of one glutathione

Received: April 19, 2013
Published: May 13, 2013

   dx.doi.org/10.1021/ja403916v | J. Am. Chem. Soc. 2013, 135, 8423−8430

ligand and covalent attachment of the $\{Fe(NO)_2\}^9$ unit within the usual glutathione binding pocket.[25]

Monomeric oxidized $\{Fe(NO)_2\}^9$ DNIC species, L(X)Fe-$(NO)_2$ or $L_2Fe(NO)_2^+$, typically display an electrochemically reversible one-electron reduction to the reduced $\{Fe(NO)_2\}^{10}$ form. A rare example of a neutral to anionic conversion, (L-L)$Fe(NO)_2$ to (L-L)$Fe(NO)_2^-$ has been successful in the case of L-L = the anionic chelating [(2,6-diisopropylphenyl)NC-(Me)]$_2$CH (Ar-nacnac) ligand.[26] Bulk chemical synthesis of the reduced species usually requires the presence of a stabilizing ligand, such as CO, PR_3, or NHCs.[7−9] In fact, transformations between the oxidized $\{Fe(NO)_2\}^9$ and the reduced $\{Fe-(NO)_2\}^{10}$ forms in biology are considered to have implications in regulating the role of the DNIC for NO storage or as an NO-release agent.[19]

We have pursued fundamental properties of synthetic DNICs of L(X)$Fe(NO)_2$ composition making use of L = imidazoles and N-heterocyclic carbenes as surrogates for protein-bound histidine donor sites.[9] Such results find that N-heterocyclic carbene ligands are the "better" ligands. They readily displace imidazoles of L(RS)$Fe(NO)_2$, leaving the $Fe(NO)_2$ unit intact, and engender stability as compared to imidazole or phosphine complexes, in the reduced $\{Fe(NO)_2\}^{10}$, oxidized $\{Fe(NO)_2\}^9$, and even the $\{Fe(NO)_3\}^{10}$ forms.[9,27]

As demonstrated in Scheme 1, we have noted a $\{Fe(NO)_2\}^9$/$\{Fe(NO)_2\}^{10}$ reduction that proceeds under extremely mild

Scheme 1. Conversion of Oxidized $\{Fe(NO)_2\}^9$ Species into Reduced $\{Fe(NO)_2\}^{10}$ in the Presence of $CO_{(g)}$.

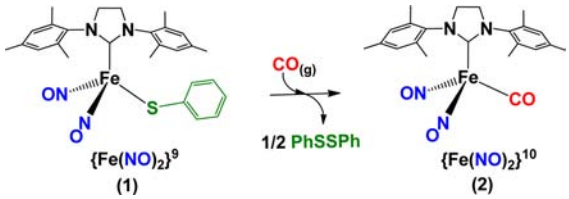

conditions and uses a thiolate/disulfide oxidation as driving force. Mechanistic details of this reaction, from experiment and theory, and a unique role of CO as initiator for RS• for the disulfide elimination are reported herein. We comment as well on an apparent parallel between the $\{Fe(NO)_2\}^9$/$\{Fe(NO)_2\}^{10}$ and d^9-Cu^{II}/d^{10}-Cu^I redox couples with regards to thiolate/disulfide interconversions.

RESULTS AND DISCUSSION

Synthesis and Characterization. Homolytic cleavage of (μ-PhS)$_2$[$Fe(NO)_2$]$_2$[28] by 2 equiv of the sIMes ligand (freshly prepared by combining 1,3- bis(2,4,6- trimethylphenyl)-imidazolinium chloride and NaO^{t}Bu in a 1:1 stoichiometric ratio) leads to the formation of complex **1**, shown in Scheme 1. This preparation is identical to that of the unsaturated NHC or IMes analogue reported earlier.[26] Reaction progress can be monitored via IR spectroscopy with notable shifts in the ν(NO) positions and pattern indicating the formation of complex **1** (ν(NO): 1763 (s), 1715(vs)) from the Roussin's red ester, (μ-PhS)$_2$[$Fe(NO)_2$]$_2$, precursor (ν(NO): 1783 (s), 1757(s)) (Figure 1). The room temperature EPR spectrum of complex **1** shows an isotropic signal at g = 2.03, the characteristic signature of the $\{Fe(NO)_2\}^9$ oxidized form of DNICs. Complex **1** is stable under inert atmosphere over several months in both solution and solid states.

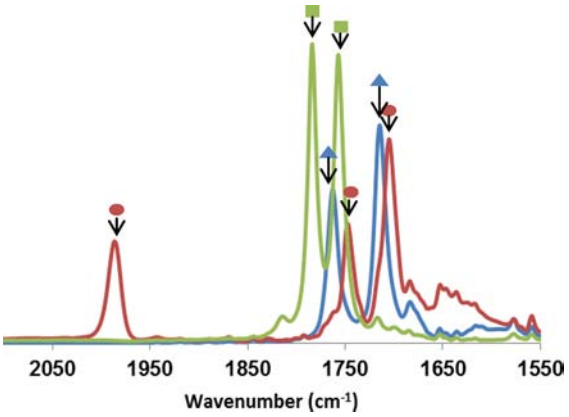

Figure 1. Overlaid IR Spectra of **RRE**, **1**, and **2** in THF [■, olive: **RRE**: ν(NO) 1783(s), 1757(s) cm^{-1}]; [▲, blue: **1**: ν(NO) 1763(s), 1715(vs) cm^{-1}]; [●, red: **2**: ν(CO) 1986(s), ν(NO) 1747(s), 1705(vs) cm^{-1}].

In the presence of $CO_{(g)}$, the oxidized, paramagnetic $\{Fe(NO)_2\}^9$ complex **1** converts to the reduced, diamagnetic $\{Fe(NO)_2\}^{10}$ complex **2**, Scheme 1. The spectral monitor indicated ν(NO) positions red-shifted by ∼15 cm^{-1} and the appearance of a new CO band at 1986 cm^{-1}, indicating the formation of the reduced DNIC **2** (Figure 1). The byproduct PhSSPh, confirmed by ^{1}H NMR and mass spectrometry,[27] is generated by bimolecular reductive elimination from **1**. The DNIC **2** is fairly air-stable in the solid state but slowly decomposes in THF solution in the presence of air at room temperature.

The DNICs **1** and **2** were obtained as dark purple and brown crystals, respectively, and their molecular structures are compared in Figure 2a,b. Both are tetrahedral complexes wherein the CN_2C_2 plane of the sIMes bisects the S−Fe−N angle of the trigonal base of **1**. This plane is aligned with one Fe−NO vector of **2**. The planes of the mesitylenes are roughly perpendicular to the CN_2C_2 plane and appear to umbrella the $Fe(NO)_2L$ motif. The average Fe−N−O angle of reduced **2** (172.7°) is slightly more linear than oxidized **1** (168.5°). The two Fe−NO are oriented in toward each other in the "attracto" conformation.[10] With the exception of the saturated ethylene linkage C−C bond, all other metrics of **1** and **2** are similar to those of the IMes analogues.[27] Table 1 lists selected bond distances and angles for **1** and **2.**

Kinetic Measurements. The rate of conversion of **1** to **2** is amenable to kinetic and mechanistic studies. This was accomplished via *in situ* IR spectroscopy of toluene solutions of **1**, saturated with CO and maintained under an atmosphere of CO. Figure 3 is a sample three-dimensional stacked plot from *in situ* IR monitoring in toluene at 333 K. The decay of the NO bands and the growth of new NO and CO bands occur at the same rate as expected for the oxidized and reduced DNICs **1** and **2**, respectively (Figure 4).

Under the conditions studied, the mole ratio of CO to DNIC in solution is approximately one to one, but, as the reaction is carried out under a CO atmosphere, the concentration of CO is constant. Under these conditions the rate was determined to have a first-order dependence with respect to the iron complex (eq 1), as evidenced by the linear natural log plot over three half-lives of the absorption data of the carbonyl band of **2** at 323 K (Figure 5). Linear plots are also observed for all NO bands giving similar k_{obs} values (see Figure S1).

dx.doi.org/10.1021/ja403916v | J. Am. Chem. Soc. 2013, 135, 8423−8430

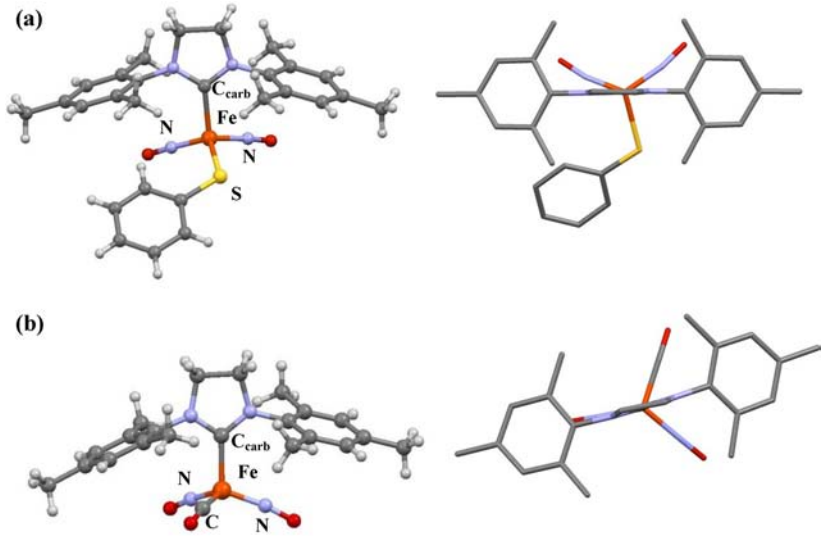

Figure 2. Molecular structures of complexes (a) **1** and (b) **2**: (left) in ball-and-stick view; (right) rotated stick views of the orientation of the NHC plane with respect to the trigonal base. Thermal ellipsoid plots and a full list of metric parameters are provided in the Supporting Information.

Table 1. Selected Bond Distances and Angles in Complexes (sIMes)Fe(NO)$_2$(SPh) 1 and (sIMes)Fe(NO)$_2$(CO) 2

	1{Fe(NO)$_2$}^{9}	**2**{Fe(NO)$_2$}^{10}
	Bond Distances (Å)	
Fe–C carb	2.048(1)	1.998(2)
Fe–NO^a	1.671(1)	1.682(2)
Fe–CO	–	1.771(2)
Fe–S	2.243(1)	–
N–O	1.174(5)	1.174(1)
	1.184(5)	1.164(1)
C–C^b	1.523(1)	1.524(1)
	Bond Angles (°)	
N–Fe–N	115.3(2)	116.6(1)
Fe–N–O^a	168.4(1)	172.7(2)
C_{carb}–Fe–NO^a	106.7(2)	109.5(1)
C_{carb}–Fe–S	109.1(1)	–
C_{carb}–Fe–CO	–	101.8(1)

^{a}Average distance or angles. ^{b}C–C distance in NHC.

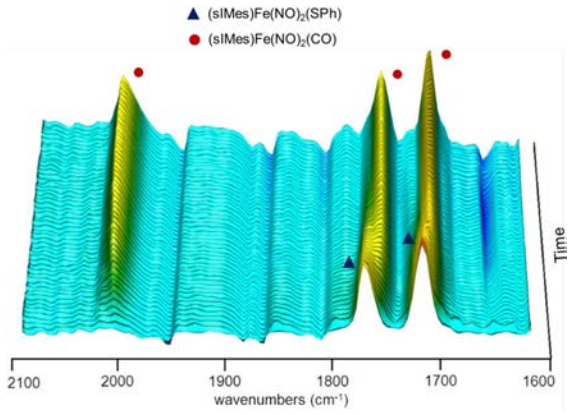

Figure 3. Three-dimensional stacked plot of the reaction of complex **1** with $CO_{(g)}$ at 333 K in toluene.

$$\text{rate} = k_{obs}[\text{Fe}]^1, \quad \text{where } k_{obs} = k[\text{CO}]^n \tag{1}$$

$$\text{rate} = k[\text{Fe}]^1[\text{CO}]^1 \tag{2}$$

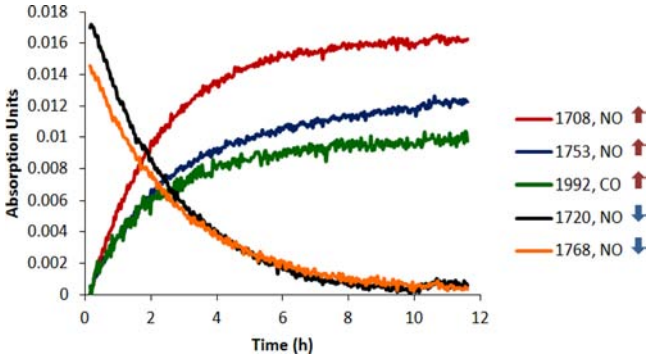

Figure 4. Reaction profiles of infrared bands for the conversion of **1** (ν(NO) 1708, 1753 cm^{-1}) to **2** (ν(CO) 1992, ν(NO) 1720, 1768 cm^{-1})) at 348 K in toluene.

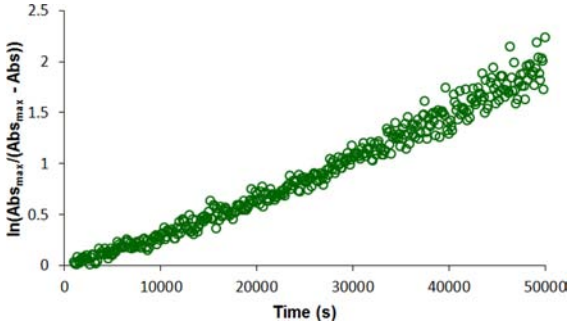

Figure 5. Natural log plot of absorption data versus time of the ν(CO) of complex **2** at 323 K. A linear trend consistent with a first-order condition in **2** gives a k_{obs} value of 4.03×10^{-5} s^{-1} calculated from the slope.

In order to establish the order of CO dependence in the rate expression in eq 1, reaction rates were monitored at CO pressures of 3.1 and 6.1 atm at 323 K. A plot of the k_{obs} vs [CO] at these pressures is linear with a y-intercept of zero implicating first-order dependence on the concentration of CO (Figure 6). The complete rate expression is thus bimolecular with a first-order rate dependence on both complex **1** and CO (eq 2).

dx.doi.org/10.1021/ja403916v | J. Am. Chem. Soc. 2013, 135, 8423–8430

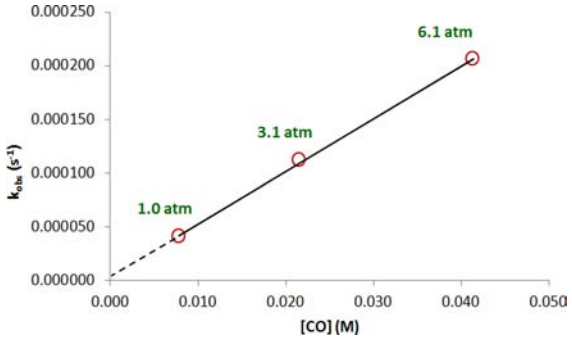

Figure 6. Plot of k_{obs} vs [CO] for the formation of complex **2** at 323 K. The R^2 value is 0.9996.

The temperature dependence of the rate constant, k, for the conversion of complex **1** to **2** was measured over a 25 K range under 1 atm of CO (Figure 7), and the resulting k values, derived as per eq 2, are listed in Table 2.

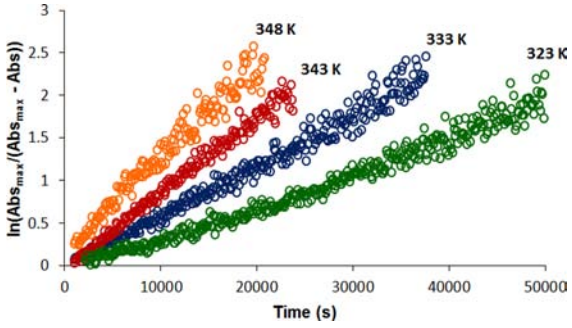

Figure 7. Natural log plots of absorption data versus time of the ν(CO) of complex **2** at various temperatures.

Table 2. Kinetic Parameters Obtained from a Linear Fit of the Natural Log Plots[a]

T (K)	k_{obs} (s^{-1})	[CO] (M)	k (M^{-1} s^{-1})
323.15	4.03×10^{-5}	0.00785	5.13×10^{-3}
333.15	6.03×10^{-5}	0.00798	7.56×10^{-3}
343.15	8.81×10^{-5}	0.00810	1.09×10^{-2}
348.15	1.09×10^{-4}	0.00816	1.34×10^{-2}

[a]CO concentrations in toluene at 1 atm were derived from literature.[29]

The activation parameters for the formation of complex **2** were determined through an Eyring analysis and found to have values for $\Delta H^{\ddagger}$ of 7.80 ± 0.16 kcal/mol and a $\Delta S^{\ddagger}$ of −45.0 ± 0.5 e.u. (Figure 8). The $\Delta G^{\ddagger}$ at 298.15 K can be calculated as 21.2 ± 0.2 kcal/mol. The small $\Delta H^{\ddagger}$ and large negative $\Delta S^{\ddagger}$ values are indicative of an associative mechanism, consistent with the second order rate expression.

Computational Results. For computational efficiency, the mesityl groups on the N-heterocyclic carbene ligand as well as the phenyl group on the thiol were replaced by CH_3 groups. The gas phase computations utilized the BP86 functional, with the 6-311+G(d,p) basis set, previously benchmarked as appropriate methodology for DNIC complexes.[30]

Mechanistic pathways consistent with the bimolecular rate expression were investigated and are presented in Figure 9. Table S5 lists the calculated electronic energies, enthalpies, and free energies of all species in Figure 9. As CO is a poor nucleophile, we explored the possibility of generating an open

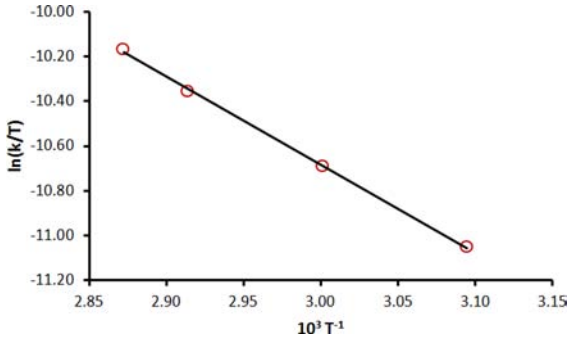

Figure 8. Eyring plot obtained from the temperature dependence of k. The R^2 value is 0.9991.

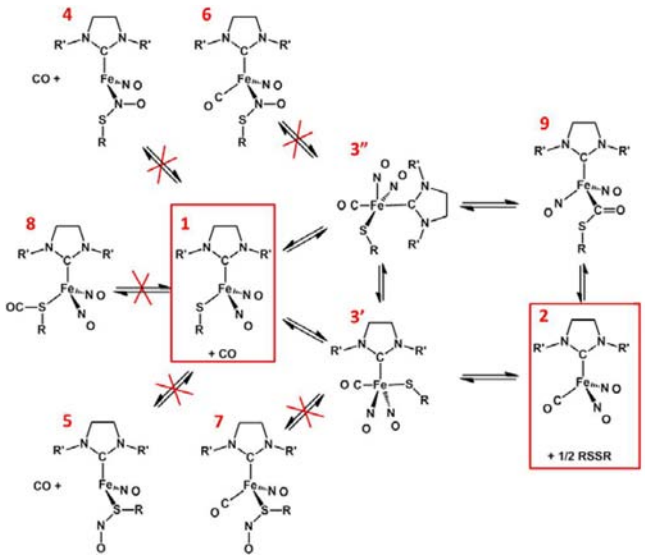

Figure 9. Structures explored as intermediates in CO addition to complex **1.** In DFT study, R = R′ = Me. In kinetics study R = Ph, R′ = Mes.

site on three-coordinate iron that might result from a rapid pre-equilibrium involving iron-bound RSNO formation. Nitrosyl insertion into the Fe−SR bond, forming an N-bound RSNO, or NO migration to the sulfur of Fe−SR, maintaining S-binding of the RSNO, yielded putative intermediates **4** and **5** in Figure 9. Neither were stable structures, and upon geometry optimization reverted to **1**. Attempts to impose such structures by constraining the S−N bond resulted in exceptionally high free energies of >36 kcal/mol, Table S5. A third possibilty considered was thiolate S/CO adduct formation, intermediate **8**, followed by CO insertion between S and Fe. However, introduction of CO at the sulfur of the Fe−SR produced neither S-CO nor Fe−C(═O)SR interactions. With such possibilities eliminated, the direct coordination of the CO, resulting in a five-coordinate iron such as intermediates **3′** and **3″**, was examined.

A five-coordinate complex like **3′** ($ML_2L'L''L'''$) could have seven isomers within the trigonal bipyramidal (tbp) geometry. Geometry optmizations of these resulted in only five stable isomers, all with similar free energies and enthalpies, Table S7. The isomers with any of the π-acid ligands (NO or CO) in both axial positions underwent a Berry pseudorotation to generate a lower energy isomer. The most stable isomer of **3′**, as shown in Figure 9, has the carbonyl and thiol ligands axial

dx.doi.org/10.1021/ja403916v | J. Am. Chem. Soc. 2013, 135, 8423−8430

largely in a tbp geometry, with a τ value of 0.75.[31] The next most stable isomer with the carbonyl and carbene in trans positions, **3″**, is only 0.2 kcal/mol higher in free energy and tending toward square pyramidal, τ = 0.31. The five-coordinate intermediates **3′** and **3″** also showed little propensity to form iron-bound RSNOs as represented by four-coordinate complexes **6** and **7**. As both **6** and **7** are computed to be higher in free energy than the experimental free energy of activation, a reaction route through either of them from **1** is unlikely. Thus, we focused on the five-coordinate intermediates **3′** and **3″** to obtain the reduced DNIC, complex **2**.

The search for transition states $[\mathbf{1}-\mathbf{3}']^{\ddagger}$ and $[\mathbf{1}-\mathbf{3}'']^{\ddagger}$ was carried out by performing a relaxed coordinate scan along the Fe−C(CO) bond, using intermediates **3′** and **3″**, respectively, as starting points. The bond under examination was stretched in 0.1 Å increments, while all other atoms were allowed to optimize. The approximate transition states at a specific Fe−C(CO) bond length were then fully optimized and characterized. Both $[\mathbf{1}-\mathbf{3}']^{\ddagger}$ or $[\mathbf{1}-\mathbf{3}'']^{\ddagger}$ were found to have similar free energies, at +19.2 and +19.6 kcal/mol respectively. (Only the $[\mathbf{1}-\mathbf{3}'']^{\ddagger}$ transition state is shown in the reaction profile, Figure 10.) These barriers are consistent with the experimentally determined free energy of activation at 25 °C, 21.2 kcal/mol. The rearrangement from **3′** to **3″** proceeds through a series of Berry pseudorotations similar in free energy to the experimental activation barrier; thus, both five-coordinate intermediates were examined for thiyl release. The free energy for direct loss of the radical thiyl from **3′** also matched the experimental value of 21.2 kcal/mol. However, a mechanism in which CO inserts into the Fe−SR bond of **3″** was found to have a lower free-energy barrier, at +18.4 kcal/mol, Figure 10. The structure of a carbonyl insertion intermediate, **9**, was located with a free energy of +10.4 kcal/mol. The tetrahedral iron coordination environment for the DNIC is thus a stabilizing force in cleaving the thiolate from the iron. From this intermediate, the homolytic C−S bond cleavage with a free-energy barrier of +17.0 kcal/mol is more facile than direct Fe−S bond cleavage. Although this proposed mechanism of SR migration or CO insertion is only valid with CO as the incoming ligand, the direct loss of the thiyl radical from **3′** is an alternative mechanism with a similar energy that may be applied to other incoming ligands. In both the direct loss of the thiyl radical and the SR/CO migratory insertion pathways, the calculated activation energy is not significantly different, and both are consistent with the experimentally observed activation energy. Our predictions also demonstrate agreement with the associative rate law, being first order in both **1** and CO. Although the thermodynamic free energy of the formation of the product, **2**, and a thiyl radical is +9.4 kcal/mol, the coupling of two thiyl radicals to form a stable disulfide produces a large driving force (ΔG = −12.8 kcal/mol) for the overall reaction.[32]

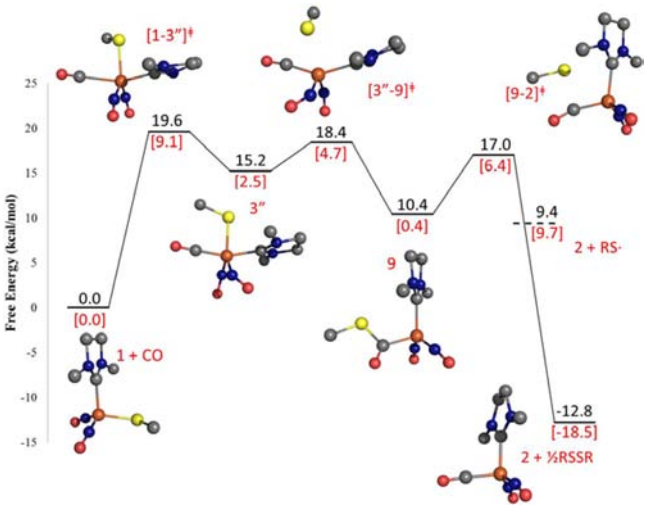

Figure 10. Lowest energy computed reaction pathway for the formation of **2**. Numbers in black are free energy; numbers in red with brackets are enthalpy.

It is instructive to consider the nature of the orbital interaction during "attack" of CO on the 17-electron complex **1** that results in the transition state $[\mathbf{1}-\mathbf{3}']^{\ddagger}$ and intermediate **3′**, especially from the perspective that CO is a poor nucleophile. Spin density plots are shown for the species with doublet states of the mechanism involving direct Fe−S bond cleavage, which is described in the reaction profile of Figure S7. The singly occupied molecular orbital (SOMO) of $[\mathbf{1}-\mathbf{3}']^{\ddagger}$ contains a σ-bonding interaction between the π^* orbital of the CO and a π orbital on the $Fe(NO)_2$ unit. Thus, it appears as if the reaction begins with the nucleophilic attack of the π-density in the N−Fe−N unit on the CO, then as the CO draws closer to the Fe, a standard σ bond is established with the expected Fe → CO π backbonding in the intermediate **3′**. In this intermediate the increased electron density on the Fe, which is now a 19-electron species, is displaced onto the NO ligands, which bend to provide better overlap of their π^* orbitals with the Fe d_{z^2}, as seen in Figure 11. The RS● radical is then lost, resulting in a stable, 18-electron system. This interpretation is supported by the bond distances listed in Figure 11. The Fe−C

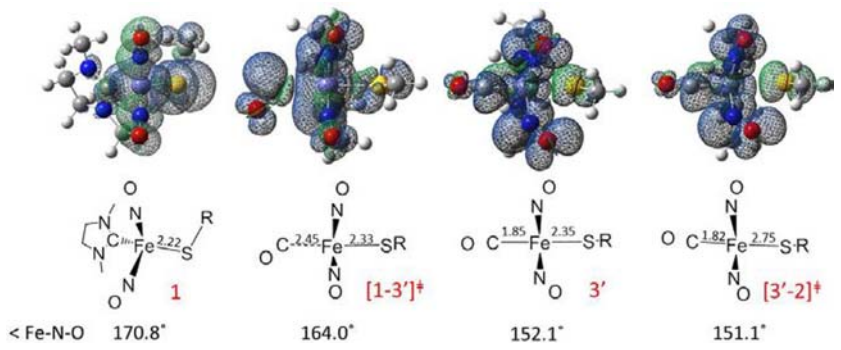

Figure 11. Spin density plots for the mechanism involving the homolytic cleavage of the Fe−S bond resulting in the loss of the thiyl radical, Figure S7, with distances in structures below. Note that the NHC ligand is behind the Fe in the five-coordinate species.

dx.doi.org/10.1021/ja403916v | J. Am. Chem. Soc. 2013, 135, 8423−8430

bond in $[1-3']^{\ddagger}$ is quite long, while the Fe−S bond has increased by only 0.1 Å from **1**. In the five-coordinate intermediate, **3′**, the Fe-CO distance has decreased by about 0.6 Å to 1.852 Å, close to that of the product, **2**. Examination of the spin density plots for both mechanisms reveals that the unpaired electron remains localized on the $Fe(NO)_2$ moiety in all intermediates and preceding transition states. If the electron were located on the S, or shared between the Fe and S, it would be appropriate to consider the compound a thiyl radical, or metal-stabilized thiyl radical, but with the $Fe(NO)_2$ unit maintaining the spin density alone, the sulfur is rightly seen as a thiolate.[33]

Further Ligand Dependence. The reaction profile suggests that $Fe(NO)_2$ transiently serves as a nucleophile toward the empty π^* orbitals of CO. This would imply an unusual dependence on ligands of better donor ability, such as phosphines. Inspired by the computational results, a preliminary study of such ligand effects was carried out. In fact, under the same solvent and monitoring conditions as was determined for CO (whose second-order rate constant is 2.4×10^{-3} $M^{-1}\cdot s^{-1}$ at 30 °C), PPh_3 was unreactive with complex **1**. Assuming this was due to steric effects, the smaller PMe_3 and $P(OMe)_3$ ligands were exposed to **1** maintaining pseudofirst-order conditions through 20-fold excesses of the ligands. From the latter reaction the $(NHC)((MeO)_3P)Fe(NO)_2$ product was identified by X-ray crystallography. The PMe_3 reaction is however complicated by NHC as well as PhS• displacement by the phosphine. Nevertheless, preliminary data indicate slower reaction rates for the better donating incoming ligands. This observation is inconsistent with typical nucleophilic substitution processes. A more extensive study of this unusual ligand effect with computational support will be the focus of a separate manuscript.

■ CONCLUSIONS

This study is centered on the relationship of thiolate-disulfide redox activity and its facilitation of the one-electron reduction of an oxidized dinitrosyl iron moiety. While stringent reductive conditions are required for the reduction of $\{Fe(NO)_2\}^9$ to $\{Fe(NO)_2\}^{10}$ in anionic $[X_2Fe(NO)_2]^-$ species,[19] in the case of neutral $L(RS)Fe(NO)_2$ (of which there are few well characterized) as explored in this study, exceedingly mild conditions effect the reduction, needing only the presence of the neutral π acceptor ligand carbon monoxide. Kinetic studies carried out on this system establish an overall second order experimental rate expression, and the activation parameters calculated thereby point toward an associative mechanism of CO substitution. Computational studies indicate a unique role for the delocalized frontier molecular orbitals of the $Fe(NO)_2$ unit whereby the entering CO ligand is initially engaged through its vacant π^* orbital. The integrity of the $Fe(NO)_2$ unit is verified throughout, permitting ligand exchange of thiolate and CO through a 5-coordinate, 19-electron intermediate with the NO ligands accommodating the excess charge. The rarely isolated 5-coordinate DNICs are known to have significantly bent Fe−N−O on the order of 155−165°,[20−22] similar to those calculated for the intermediate **3′**, 146° and 158°.

Thiolate-disulfide redox processes are of extensive chemical and biological relevance. Limited reports of thiolate-disulfide reactivity in an inorganic context include a kinetic study by McAuley et al.,[34] that concentrates on the oxidation of 2-mercaptosuccinic acid by Cu^{II} ions, ultimately yielding the disulfide and a Cu^{I} dimer. Formation of the disulfide is said to be facilitated by the dimer template. Similarly, Henkel et al. reported on chloride ion induced thiolate-disulfide conversion concomitant with Cu^{II}/Cu^{I} redox activity, again taking place on a dithiolate ligand scaffold bound to copper.[35] Copper(II) is known to be a potent oxidant for disulfide formation in proteins. Among many reports is that of a suggested role for such Cu-facilitated disulfide formation in the maturation process of the superoxide dismutase 1, SOD1. A copper chaperone superoxide dismutase, CCS, is proposed to assemble cysteinyl thiolates resulting in disulfides between the CCS and the apo-Cu-SOD1, ultimately leading to the translocation of copper into the SOD1.[36]

There is an obvious correlation between the two redox levels of the DNICs, $\{Fe(NO)_2\}^9/\{Fe(NO)_2\}^{10}$ and the two redox levels of copper (Cu^{II}:d^9/Cu^{I}:d^{10}). Given this, the occurrence of analogous reactivity patterns involving thiolate/disulfide reactivity between the $\{Fe(NO)_2\}^9/\{Fe(NO)_2\}^{10}$ and Cu^{II}/Cu^{I} systems could be viewed as probable. Even structural studies have shown similarities. For example, we and others have observed the formation of tetrameric, imidazolate-bridged DNIC, $\{Fe(NO)_2\}^9$ structures,[37,38] that are analogous to imidazolate-bridged tetracopper, Cu^{II}, d^9, molecular squares.[39,40]

Major questions exist regarding the roles of NO and CO as diatomic ligands in biology and physiology. In fact, even the possibility that these ligands might appear together in biological milieu has received some notice.[41] Carbon monoxide, derived from heme oxygenase 1 or 2 is reported to stimulate the nitric oxide synthase-NO pathway, reinforcing NO production.[41] Hence, on two levels of chemical features of biological significance, our study of CO-induced disulfide elimination from a dinitrosyl iron thiolate might be taken as a potential model for intracellular, thiol-complexed DNICs, exposed to intracellular CO, inducing redox level changes at iron, and attendant spectroscopic and reactivity properties.

■ EXPERIMENTAL SECTION

General Methods and Materials. Solvents were reagent grade, further purified and degassed by a Bruker solvent purification system, and stored over molecular sieves. Reagents, including 1,3-bis(2,4,6-trimethylphenyl)imidazolinium chloride ($sIMesH^+Cl^-$) and sodium *tert*-butoxide were purchased from Sigma-Aldrich Chemical Co. and were used as received. Standard Schlenk-line techniques (N_2 atmosphere) and an Ar-filled glovebox were used to maintain anaerobic conditions during preparation, isolation, and product storage. Roussin's red ester $(\mu\text{-SPh})_2[Fe(NO)_2]_2$ was prepared according to published procedures.[28]

Physical Measurements. Infrared spectra of reagents and products were recorded on a Bruker Tensor 27 FTIR spectrometer in CaF_2 solution cells of 0.1 mm path length. Elemental analyses of crystalline samples were determined by Atlantic Microlab, Inc., Norcross, GA. EPR spectra were recorded in THF using a Bruker ESP 300 equipped with an Oxford ER910 cryostat operating at 298 K. ^1H NMR spectra were recorded in $CDCl_3$ (complex **2**) and CD_2Cl_2 (PhSSPh) using a Mercury 300 MHz NMR spectrometer.

X-ray Crystallography. A Bausch and Lomb 10× microscope was used to identify suitable crystals of the same habit. Each crystal was coated in paratone, affixed to a Nylon loop, and placed under streaming nitrogen (110K) in a SMART Apex CCD diffractometer (see details in Supporting Information .cif files). The space groups were determined on the basis of systematic absences and intensity statistics. The structures were solved by direct methods and refined by full-matrix least-squares on F^2. Anisotropic displacement parameters were determined for all nonhydrogen atoms. Hydrogen atoms were placed at idealized positions and refined with fixed isotropic

dx.doi.org/10.1021/ja403916v | J. Am. Chem. Soc. 2013, 135, 8423−8430

displacement parameters. The following is a list of programs used: data collection and cell refinement, APEX2;[42] data reductions, SAINT-PLUS version 6.63;[43] absorption correction, SADABAS;[44] structural solutions, SHELXS-97;[45] structural refinement, SHELXL-97;[46] graphics and publication materials, Mercury version 2.3.[47]

*Synthesis of (sIMes)Fe(NO)$_2$(SPh) (**1**).* A 0.27 g (0.80 mmol) sample of 1,3-bis(2,4,6-trimethylphenyl)imidazolinium chloride and 0.12 g (1.2 mmol) of NaOtBu were dissolved in 20 mL of THF and stirred for 30 min prior to transfer to a Schlenk flask containing 1.0 mmol of the Roussin's red ester (μ-SPh)$_2$[Fe(NO)$_2$]$_2$ in 10 mL of THF. Stirring for 30 min resulted in a deep purple solution, which was then dried *in vacuo*. The resulting dark purple residue (>90% yield) was dissolved in 10 mL of ether and filtered through Celite. The filtrate was dried and redissolved in THF. X-ray quality crystals were grown from concentrated Et$_2$O solution at 0 °C. IR (THF, cm^{-1}) ν(NO) 1763(s), 1715(vs). Elemental anal. calcd for $FeC_{27}H_{31}N_4O_2S$ (found): C, 61.02 (61.08); H, 5.88 (5.98); N, 10.54 (10.33).

*Reaction of 1 with CO(g) To Give (sIMes)Fe(NO)$_2$(CO) (**2**).* Carbon monoxide was bubbled into a 20 mL THF solution of complex **1** (~0.5 mmol) in a 100 mL Schlenk flask for 10 min. The flask was sealed under 1 atm $CO_{(g)}$, and the solution was stirred overnight at room temperature. The formation of complex **2** was monitored by IR spectroscopy. A brown colored product was obtained in high yield (>90%). X-ray quality crystals were obtained from concentrated Et$_2$O solution at 0 °C. IR (THF, cm^{-1}) ν(CO) 1986(vs), ν(NO) 1747(s), 1705(s). Elemental anal. calcd for $FeC_{22}H_{26}N_4O_3$ (found): C, 58.68 (59.18); H, 5.82 (5.96); N, 12.44 (12.17). ^{1}H NMR ($CDCl_3$): δ 6.96 (s, aromatic H on Mes), 4.01 (s, NCH_2), 2.29 (*s*, *o*, *m*, *p*-CH_3 on Mes). The diphenyl disulfide formed as the byproduct of the above reaction was characterized by ^{1}H NMR spectroscopy. ^{1}H NMR (CD_2Cl_2): PhSSPh δ 7.53(d, SCCH), 7.27 (m); $FeC_{22}H_{26}N_4O_3$ δ 6.98 (s, aromatic H on Mes), 4.02 (s, NCH_2), 2.29 (*s*, *o*, *m*, *p*-CH_3 on mes).

A NMR spectrum was also obtained of a sample of pure $FeC_{22}H_{26}N_4O_3$ (complex **1**) spiked with pure PhSSPh for comparison (see Supporting Information).

Kinetic Measurements. *In situ* infrared monitoring was carried out using a Mettler Toledo iC10 ReactIR with an AgX fiber conduit probe having a SiComp ATR crystal. In a typical experiment, a 0.010 M solution of (sIMes)Fe(NO)$_2$(SPh) (**1**) was prepared in a 250 mL three-neck round-bottom flask fitted with the probe by dissolving the compound with 5 mL of CO-saturated toluene under an atmosphere of CO. Once completely dissolved (within 30 s of stirring), the FTIR monitoring was started, and the reaction followed until completion. Figure S6 shows a picture of the experimental setup. The reactions were conducted over a temperature range from 323 to 348 K; the solubility data of CO was obtained from extrapolation of data in literature.[29,48] The high-pressure CO reactions were monitored using an ASI ReactIR 1000 reaction analyses system with a stainless steel Parr autoclave modified with a permanently mounted ATR crystal (SiComp) at the bottom of the reactor (purchased from Mettler Toledo).

Computational Methodology. Geometry optimizations and frequency calculations were performed in the gas phase utilizing the BP86 functional[49,50] with the 6-311+G(d,p) basis set,[51−54] as previously demonstrated to be a suitable combination that best describes the electronic and vibrational structure of dinitrosyl iron complexes.[30] Where possible, geometries were obtained from crystallographic coordinates and utilized as starting geometries for optimizations. Enthalpy and free energy corrections to the electronic energy of all stable geometries were calculated at 298.15 K by Gaussian09,[55] where all energies were obtained in hartrees, then converted to kilocalories per mole. These calculated complexes matched closely with the experimental data provided by X-ray crystallography as well as the ν(NO) and ν(CO) IR stretching modes. For computational efficiency, the mesityl groups of the NHC and phenyl group of SPh were replaced by CH_3. All stable geometries had no imaginary vibrational modes, while transition states were located with a single imaginary mode. The Ampac Graphical User Interface (AGUI) program was used to extract geometric data as well as infrared frequency and bending and stretching vector data.

■ ASSOCIATED CONTENT

Ⓢ Supporting Information

Additional spectroscopic, kinetic and computational details, X-ray crystallographic data (CIF) from the structure determination and full list of metric parameters for complexes **1** and **2**. This material is available free of charge via the Internet at http://pubs.acs.org.

■ AUTHOR INFORMATION

Corresponding Author

marcetta@mail.chem.tamu.edu

Author Contributions

†These authors contributed equally.

Notes

The authors declare no competing financial interest.

■ ACKNOWLEDGMENTS

We are thankful for financial support from the National Science Foundation (CHE-0910679 to M.Y.D., CHE-1057743 to D.J.D., and CHE-0910552 to M.B.H.), and the Robert A. Welch Foundation (A-0294 to M.Y.D., A-0293 to D.J.D., and A-0648 to M.B.H.). The authors acknowledge the Laboratory for Molecular Simulation at Texas A&M University for providing computing resources.

■ REFERENCES

(1) Vanin, A. F. *Nitric Oxide* **2009**, *21*, 1−13.
(2) Hayton, T. W.; Legzdins, P.; Sharp, W. B. *Chem. Rev.* **2002**, *102*, 935−992.
(3) Ford, P. C.; Lorkovic, I. M. *Chem. Rev.* **2002**, *102*, 993−1018.
(4) Tonzetich, Z. J.; Héroguel, F.; Do, L. H.; Lippard, S. J. *Inorg. Chem.* **2011**, *50*, 1570−1579.
(5) Butler, A. R.; Megson, I. L. *Chem. Rev.* **2002**, *102*, 1155−1166.
(6) Tsai, M.-L.; Hsieh, C.-H.; Liaw, W.-F. *Inorg. Chem.* **2007**, *46*, 5110−5117.
(7) McBride, D. W.; Stafford, S. L.; Stone, F. G. A. *Inorg. Chem.* **1962**, *1*, 386−388.
(8) Atkinson, F. L.; Blackwell, H. E.; Brown, N. C.; Connelly, N. G.; Crossley, J. G.; Orpen, A. G.; Rieger, A. L.; Rieger, P. H. *J. Chem. Soc., Dalton Trans.* **1996**, 3491−3502.
(9) Hess, J. L.; Hsieh, C.-H.; Reibenspies, J. H.; Darensbourg, M. Y. *Inorg. Chem.* **2011**, *50*, 8541−8552.
(10) Reginato, N.; McCrory, C. T. C.; Pervitsky, D.; Li, L. *J. Am. Chem. Soc.* **1999**, *121*, 10217−10218.
(11) Boese, M.; Mordvintcev, P. I.; Vanin, A. F.; Busse, R.; Mulsch, A. *J. Biol. Chem.* **1995**, *270*, 29244−29249.
(12) Ding, H.; Demple, B. *Proc. Natl. Acad. Sci. U.S.A.* **2000**, *97*, 5146−5150.
(13) Enemark, J. H.; Feltham, R. D. *Coord. Chem. Rev.* **1974**, *13*, 339−406.
(14) Rahmanto, Y. S.; Kalinowski, D. S.; Lane, D. J. R.; Lok, H. C.; Richardson, V.; Richardson, D. R. *J. Biol. Chem.* **2012**, *287*, 6960−6968.
(15) Hickok, J. R.; Sahni, S.; Shen, H.; Arvind, A.; Antoniou, C.; Fung, L. W. M.; Thomas, D. D. *Free Radical Biol. Med.* **2011**, *51*, 1558−1566.
(16) Tomson, N. C.; Crimmin, M. R.; Petrenko, T.; Rosebrugh, L. E.; Sproules, S.; Boyd, W. C.; Bergman, R. G.; DeBeer, S.; Toste, F. D.; Wieghardt, K. *J. Am. Chem. Soc.* **2011**, *133*, 18785−18801.
(17) Ye, S.; Neese, F. *J. Am. Chem. Soc.* **2010**, *132*, 3646−3647.
(18) Hsieh, C.-H.; Brothers, S. M.; Reibenspies, J. H.; Hall, M. B.; Popescu, C. V.; Darensbourg, M. Y. *Inorg. Chem.* **2013**, *52*, 2119−2124.
(19) Tsai, F.-T.; Chiou, S.-J.; Tsai, M.-C.; Tsai, M.-L.; Huang, H.-W.; Chiang, M.-H.; Liaw, W.-F. *Inorg. Chem.* **2005**, *44*, 5872−5881.

(20) Chen, C.-H.; Ho, Y.-C.; Lee, G.-H. *J. Organomet. Chem.* **2009**, *694*, 3395−3400.
(21) Jo, D.-H.; Chiou, Y.-M.; Que, L. *Inorg. Chem.* **2001**, *40*, 3181−3190.
(22) Shih, W.-C.; Lu, T.-T.; Yang, L.-B.; Tsai, F.-T.; Chiang, M.-H.; Lee, J.-F.; Chiang, Y.-W.; Liaw, W.-F. *J. Inorg. Biochem.* **2012**, *113*, 83−93.
(23) Tsai, M.-L.; Chen, C.-C.; Hsu, I. J.; Ke, S.-C.; Hsieh, C.-H.; Chiang, K.-A.; Lee, G.-H.; Wang, Y.; Chen, J.-M.; Lee, J.-F.; Liaw, W.-F. *Inorg. Chem.* **2004**, *43*, 5159−5167.
(24) Chang, H.-H.; Huang, H.-J.; Ho, Y.-L.; Wen, Y.-D.; Huang, W.-N.; Chiou, S.-J. *Dalton Trans.* **2009**, 6396−6402.
(25) Cesareo, E.; Parker, L. J.; Pedersen, J. Z.; Nuccetelli, M.; Mazzetti, A. P.; Pastore, A.; Federici, G.; Caccuri, A. M.; Ricci, G.; Adams, J. J.; Parker, M. W.; Lo Bello, M. *J. Biol. Chem.* **2005**, *280*, 42172−42180.
(26) Tonzetich, Z. J.; Do, L. H.; Stephen J. Lippard, S. J. *J. Am. Chem. Soc.* **2009**, *131*, 7964−7965.
(27) Hsieh, C.-H.; Darensbourg, M. Y. *J. Am. Chem. Soc.* **2010**, *132*, 14118−14125.
(28) Rauchfuss, T. B.; Weatherill, T. D. *Inorg. Chem.* **1982**, *21*, 827−830.
(29) Field, L. R.; Wilhelm, E.; Battino, R. *J. Chem. Thermodyn.* **1974**, *6*, 237−243.
(30) Brothers, S. M.; Darensbourg, M. Y.; Hall, M. B. *Inorg. Chem.* **2011**, *50*, 8532−8540.
(31) Addison, A. W.; Rao, T. N.; Reedijk, J.; van Rijn, J.; Verschoor, G. C. *J. Chem. Soc., Dalton Trans.* **1984**, 1349−1356.
(32) Melzer, M. M.; Mossin, S.; Cardenas, A. J. P.; Williams, K. D.; Zhang, S.; Meyer, K.; Warren, T. H. *Inorg. Chem.* **2012**, *51*, 8658−8660.
(33) Ouch, K.; Mashuta, M. S.; Grapperhaus, C. A. *Inorg. Chem.* **2011**, *50*, 9904−9914.
(34) Lappin, A. G.; McAuley, A. *J. Chem. Soc., Dalton Trans.* **1978**, 1606−1609.
(35) Neuba, A.; Haase, R.; Meyer-Klaucke, W.; Flörke, U.; Henkel, G. *Angew. Chem., Int. Ed.* **2012**, *51*, 1714−1718.
(36) Furukawa, Y.; Torres, A. S.; O'Halloran, T. V. *EMBO J.* **2004**, *23*, 2872−2881.
(37) Hess, J. L.; Hsieh, C. H.; Brothers, S. M.; Hall, M. B.; Darensbourg, M. Y. *J. Am. Chem. Soc.* **2011**, *133*, 20426−20434.
(38) Wang, X.; Sundberg, E. B.; Li, L.; Kantardjieff, K. A.; Herron, S. R.; Lim, M.; Ford, P. C. *Chem. Commun.* **2005**, 477−479.
(39) Chaudhuri, P.; Karpenstein, I.; Winter, M.; Lengen, M.; Butzlaff, C.; Bill, E.; Trautwein, A. X.; Floerke, U.; Haupt, H. J. *Inorg. Chem.* **1993**, *32*, 888−894.
(40) Kolks, G.; Lippard, S. J.; Waszczak, J. V.; Lilienthal, H. R. *J. Am. Chem. Soc.* **1982**, *104*, 717−725.
(41) Motterlini, R.; Otterbein, L. E. *Nat. Rev. Drug Discovery* **2010**, *9*, 728−743.
(42) *APEX2*, version 2009.7−0; Bruker AXS Inc.: Madison, WI, 2007.
(43) *SAINTPLUS: Program for Reduction of Area Detector Data*, version 6.63; Bruker AXS Inc.: Madison, WI, 2007.
(44) Sheldrick, G. M. *SADABS: Program for Absorption Correction of Area Detector Frames*; Bruker AXS Inc.: Madison, WI, 2001.
(45) Sheldrick, G. M. *SHELXS-97: Program for Crystal Structure Solution*; Universität Göttingen: Göttingen, Germany, 1997.
(46) Sheldrick, G. M. *SHELXL-97: Program for Crystal Structure Refinement*; Universität Göttingen: Göttingen, Germany, 1997.
(47) Mercury: Macrae, C. F.; Edgington, P. R.; McCabe, P.; Pidcock, E.; Shields, G. P.; Taylor, R.; Towler, M.; van de Streek, J. *J. Appl. Crystallogr.* **2006**, *39*, 453−457.
(48) Park, J.; Yi, X.; Gasem, K. A. M.; Robinson, R. L., Jr. *J. Chem. Eng. Data* **1995**, *40*, 245−247.
(49) Becke, A. D. *Phys. Rev. A* **1988**, *38*, 3098−3100.
(50) Perdew, J. P. *Phys. Rev. B* **1986**, *33*, 8822−8824.
(51) Krishnan, R.; Binkley, J. S.; Seeger, R.; Pople, J. A. *J. Chem. Phys.* **1980**, *72*, 650−654.
(52) Wachters, A. J. H. *J. Chem. Phys.* **1970**, *52*, 1033−1036.
(53) Hay, P. J. *J. Chem. Phys.* **1977**, *66*, 4377−4384.
(54) Raghavachari, K.; Trucks, G. W. *J. Chem. Phys.* **1989**, *91*, 1062−1065.
(55) Frisch, M. J.; Trucks, G. W.; Schlegel, H. B.; Scuseria, G. E.; Robb, M. A.; Cheeseman, J. R.; Scalmani, G.; Barone, V.; Mennucci, B.; Petersson, G. A.; Nakatsuji, H.; Caricato, M.; Li, X.; Hratchian, H. P.; Izmaylov, A. F.; Bloino, J.; Zheng, G.; Sonnenberg, J. L.; Hada, M.; Ehara, M.; Toyota, K.; Fukuda, R.; Hasegawa, J.; Ishida, M.; Nakajima, T.; Honda, Y.; Kitao, O.; Nakai, H.; Vreven, T.; Montgomery, J. A., Jr.; Peralta, J. E.; Ogliaro, F.; Bearpark, M.; Heyd, J. J.; Brothers, E.; Kudin, K. N.; Staroverov, V. N.; Kobayashi, R.; Normand, J.; Raghavachari, K.; Rendell, A.; Burant, J. C.; Iyengar, S. S.; Tomasi, J.; Cossi, M.; Rega, N.; Millam, J. M.; Klene, M.; Knox, J. E.; Cross, J. B.; Bakken, V.; Adamo, C.; Jaramillo, J.; Gomperts, R.; Stratmann, R. E.; Yazyev, O.; Austin, A. J.; Cammi, R.; Pomelli, C.; Ochterski, J. W.; Martin, R. L.; Morokuma, K.; Zakrzewski, V. G.; Voth, G. A.; Salvador, P.; Dannenberg, J. J.; Dapprich, S.; Daniels, A. D.; Farkas, Ö.; Foresman, J. B.; Ortiz, J. V.; Cioslowski, J.; Fox, D. J. *Gaussian 09*, revision B.01, Gaussian, Inc.: Wallingford, CT, 2009.